

# Third-order response of metallic acGNR to an elliptically-polarized terahertz excitation field

Yichao Wang<sup>1</sup> and David R. Andersen<sup>1,2</sup>

<sup>1</sup>*Electrical and Computer Engineering*

<sup>2</sup>*Physics and Astronomy*

*The University of Iowa, Iowa City, IA 52242 USA*

(Dated: Jun. 15, 2016)

## Abstract

We present a theoretical description of the third-order response induced by an elliptically-polarized terahertz beam normally-incident on intrinsic and extrinsic metallic armchair graphene nanoribbons. Our results show that using a straightforward experimental setup, it should be possible to observe novel polarization-dependent nonlinearities at low excitation field strengths of the order of  $10^4$  V/m. At low temperatures the Kerr nonlinearities in extrinsic nanoribbons persist to significantly higher excitation frequencies than they do for linear polarizations, and at room temperatures, the third-harmonic nonlinearities are enhanced by 2-3 orders of magnitude. Finally, the Fermi-level and temperature dependence of the nonlinear response is characterized.

Graphene is a flat monolayer of carbon atoms tightly packed into a 2D honeycomb lattice. Graphene has emerged to be a very promising candidate for terahertz (THz) applications, and opens up the possibility of graphene based devices for THz optoelectronic and photonic applications [1]. Theoretical and experimental studies show that unique properties of graphene, such as linear dispersion relation near the Dirac point, high electron Fermi velocity, and tunable Fermi level lead to a strong nonlinear response in 2D graphene structures and suggest it is a very promising candidate for THz applications [1–12]. This work opens up the possibility of graphene based devices for THz optoelectronic and photonic applications [1, 13].

Following the first experimental study of absorption in the ellipsometric spectrum of graphene [14], the circular AC Hall effect [15–17], chiral edge currents [18, 19], helicity-dependent photovoltaic Hall effect [1, 15] and electronic chirality and Berry phases [20] were observed by using circularly-polarized excitation fields. Higher-order harmonic generation [5, 21] in 2D graphene has also been theoretically investigated, showing strong higher-order harmonics exist in graphene with an applied circularly-polarized harmonic electric field. This work shows that elliptically- or circularly-polarized light may be used to probe the unique nature of graphene near the Dirac points, including effects such as harmonic generation, frequency mixing, optical rectification, linear and circular photogalvanic effect, photon drag, photoconductivity, coherently controlled ballistic charge currents, pseudospin, chirality, and symmetry breaking [1, 5, 14–17, 19, 20].

In general, graphene nanoribbons (GNRs) have two types of edges: armchair edges (acGNR) and zigzag edges (zzGNR). Due to the geometry and boundary conditions [22–24], these two types of GNRs show distinct electronic characteristics in the low energy regime. The linear and nonlinear response of GNRs due to a linearly-polarized electric field were studied in [25–31]. The non-perturbative DC conductance due to an applied circularly-polarized field in zzGNR and acGNR [28, 29] was also investigated. However, there has been no investigation of the nonlinear response in metallic acGNR for an elliptically polarized applied electric field.

In this Letter, we describe new results on the nonlinear response of intrinsic and extrinsic metallic acGNR (mGNR) excited by a normally-incident, *elliptically-polarized* THz electric field. GNR are metallic in the  $\mathbf{k} \cdot \mathbf{p}$  approximation when the longitudinal direction ( $\hat{y}$ ) of the nanoribbon is parallel to the armchair edge and the nanoribbon atomic width is

$N = (3M - 1)$  with  $M$  odd. In this case the lowest sub-bands are linear in  $k_y$ , and for sufficiently narrow mGNRs ( $L_x < \sim 20$  nm), the higher sub-bands are far enough away that their contributions to the THz nonlinear conductance may be neglected. *Most significantly*, we show that at room temperature, the third-order nonlinear conductance at  $3\omega$  is enhanced by 2 – 3 orders of magnitude using a circularly-polarized (CP) THz field over the same conductance when the excitation field is linearly-polarized (LP)[30]. We also show that the third-order conductances at  $\omega$  and  $3\omega$  exhibit odd symmetry in the polarization state, resulting in current densities of opposite sign for opposite-handed elliptical polarizations. Finally, we analyze the Fermi level and temperature dependence of these nonlinearities and show that by varying the polarization state of the excitation field it is possible to tune the nonlinearities in both sign and amplitude. This novel behavior suggests a variety of applications in optical modulation, polarization switching, and harmonic generation over the THz region of the optical spectrum.

Our  $\mathbf{k} \cdot \mathbf{p}$  model employs Fourier analysis to solve the nonlinear Dirac equation using time-dependent perturbation theory in order to study the *polarization-dependent* nonlinear response in the THz regime. The model is an extension of one first applied by us in the context of graphene nanoribbons for the study of nonlinear effects induced by LP THz fields [30, 31]. However, we emphasize that the work presented below contains new physics as a result of the coupling between the polarization state of the incident field and the chiral mGNR wavefunctions, and is not a simple superposition of the previous description of LP THz excitations (although the previous results do exist as special cases of the current work).

In the following, we analyze nonlinear harmonic generation at THz frequencies induced by an elliptically-polarized beam normally-incident on a mGNR. The polarization ellipse is characterized by major and minor axes that coincide with the longitudinal and transverse axes of the nanoribbon. This polarization state can be achieved experimentally by passing a  $\hat{y}$ -polarized beam through a cascade of a half-wave plate oriented with its fast axis at an angle  $\phi/2$  with respect to the polarization axis of the incident THz beam, and then through a quarter-wave plate oriented with its principle axes parallel to the longitudinal ( $\hat{y}$ ) and transverse ( $\hat{x}$ ) axes of the mGNR. The corresponding electric field may be expressed as  $\mathbf{E} = [i\hat{x}E_x + \hat{y}E_y] \exp[-i\omega t] = E_0 [i\hat{x} \sin(\phi) + \hat{y} \cos(\phi)] \exp[-i\omega t]$ .

We begin by writing the polarization state of an elliptically-polarized beam with principal axes parallel to  $\hat{x}$  and  $\hat{y}$ . In the Coulomb gauge for a source-free region of constant scalar

potential ( $\nabla\varphi = 0$ ), the time-harmonic electric field turns on adiabatically at  $t_0 = -\infty$  and the magnetic vector potential is  $\mathbf{A} = \mathbf{E}/(i\omega)$ . After making the substitution,  $\mathbf{k}(\mathbf{k}') \rightarrow \mathbf{k}(\mathbf{k}') + q\mathbf{A}/\hbar$ , we obtain a time and polarization-state dependent Hamiltonian  $H$  near the Dirac points of the mGNR [30, 31]. The Fourier expansion of the resulting perturbation wave function is written:

$$\psi(\mathbf{r}, t; m) = \sum_{l=0}^{\infty} \psi_0(m, l) \exp[i2\pi m y/L_y] \exp[-i\omega l t] \exp[-i\epsilon t/\hbar]$$

where  $m$  is the quantum number of  $k_y$ ,  $l$  is the harmonic order of the electric field, and  $\psi_0(m, l)$  is a spinor of order  $(m, l)$ . Following Ref. [1, 2, 11, 12, 30], we obtain the third order current density in the perturbation limit, with  $\omega_y = v_F 2\pi m/L_y$ :

$$\begin{aligned} J_\nu^{(3)}(\phi, t) &= \sum_{\alpha\beta\gamma} \left[ \exp[-i\omega t] \sigma_{\nu\alpha\beta\gamma}^{(3)}(\omega, -\omega, \omega) E_\alpha E_\beta^* E_\gamma \right. \\ &\quad + \exp[-i\omega t] \sigma_{\nu\alpha\beta\gamma}^{(3)}(\omega, \omega, -\omega) E_\alpha E_\beta E_\gamma^* \\ &\quad \left. + \exp[-i3\omega t] \sigma_{\nu\alpha\beta\gamma}^{(3)}(\omega, \omega, \omega) E_\alpha E_\beta E_\gamma \right] + c.c. \end{aligned} \quad (1a)$$

$$\begin{aligned} &= e g_s g_v \sum_m \left[ \psi_0(m, 1)^\dagger \frac{\partial H}{\hbar \partial k_\nu} \psi_0(m, 2) \exp[-i\omega t] \right. \\ &\quad \left. + \psi_0(m, 0)^\dagger \frac{\partial H}{\hbar \partial k_\nu} \psi_0(m, 3) \exp[-i3\omega t] \right] N(\omega_y) + c.c. \end{aligned} \quad (1b)$$

$$\begin{aligned} &= [g_\nu^{(3)}(\omega, \phi) \exp[-i\omega t] \\ &\quad + g_\nu^{(3)}(3\omega, \phi) \exp[-i3\omega t]] E_0 + c.c. \end{aligned} \quad (1c)$$

with the thermal factor defined as:

$$N(\omega_y) = \frac{\sinh\left(\frac{\hbar|\omega_y|}{k_B T}\right)}{\cosh\left(\frac{E_F}{k_B T}\right) + \cosh\left(\frac{\hbar|\omega_y|}{k_B T}\right)} \quad (2)$$

with  $\nu = x, y$  indicating the induced optical current component in the  $\hat{\nu}$  direction. The longitudinal Kerr conductance  $g_\nu^{(3)}(\omega, \phi)$  and third-harmonic conductance  $g_\nu^{(3)}(3\omega, \phi)$  for infinitely-long mGNR:

$$g_y^{(3)}(\omega, \phi) = g_0 \left[ f(\phi, -2, -1) N\left(\frac{\omega}{2}\right) + f(\phi, -1, -\frac{3}{2}) N(\omega) \right] \quad (3a)$$

$$\begin{aligned} g_y^{(3)}(3\omega, \phi, \lambda) &= g_0 \left[ f(\phi, \frac{1}{2}, -\frac{1}{24}) N\left(\frac{\omega}{2}\right) - f(\phi, 1, \frac{5}{6}) N(\omega) \right. \\ &\quad \left. + f(\phi, \frac{1}{2}, \frac{7}{8}) N\left(\frac{3\omega}{2}\right) \right] \end{aligned} \quad (3b)$$

and the transverse third-order conductances:

$$g_x^{(3)}(\omega, \phi) = g_0 \left[ f\left(\phi, 1, -\frac{1}{2}\right) N(\omega) \right] \quad (4a)$$

$$g_x^{(3)}(3\omega, \phi, \lambda) = g_0 \left[ -f\left(\phi, \frac{1}{2}, -\frac{5}{24}\right) N\left(\frac{\omega}{2}\right) + f\left(\phi, 1, \frac{1}{6}\right) N(\omega) - f\left(\phi, \frac{1}{2}, \frac{7}{8}\right) N\left(\frac{3\omega}{2}\right) \right] \quad (4b)$$

where  $f(\phi, a, b) = \eta\eta_x \cos(\phi) [a \cos^2(\phi) + 2b \sin^2(\phi)]$ ,  $g_0 = e^2/(4\hbar^2)$ , Fermi level  $E_F$ ,  $\eta_x = (g_s g_v v_F)/(\omega L_x)$ , and  $\eta = (e^2 E_0^2 v_F^2)/(\hbar^2 \omega^4)$ . It is worth noting that for a circularly-polarized excitation field, a symmetry-breaking occurs in 2D SLG that allows second-harmonic generation to occur [1, 5, 11]. We will discuss how this symmetry-breaking affects second-harmonic generation in mGNR in a future paper.

In Eqs. (3a) and (4a),  $E_0 f(\phi, a, b)$  may be split into two terms:

$$E_0 f(\phi, a, b) = f_A(\phi, a) |E_y|^2 E_y + f_B(\phi, b) P_{circ} E_x,$$

where the radiation helicity  $P_{circ} = i [E_y (iE_x)^* - iE_x E_y^*] = E_0^2 \sin(2\phi)$  [18].  $f_A(\phi, a)$  defines the conductivity tensor element  $\sigma_{\nu yyy}^{(3)}$  and  $f_B(\phi, b)$  defines the sum of conductivity tensor elements  $\sum_{yxx} \sigma_{\nu yxx}^{(3)}$ , where  $\sum_{yxx}$  indicates the sum over the rotation of indices  $\nu yxx$ ,  $\nu xyx$ , and  $\nu xxy$ . We summarize the tensor elements obtained from Eqs. (3a) and (4a) in Table I.

TABLE I. Kerr conductivity tensor elements

single-photon ( $-\omega/2 \rightarrow \omega/2$ ) conductivity element(s)	value ( $\times g_0\eta\eta_x/E_0^2$ )
$\sigma_{yyyy}^{(3)}(\omega, -\omega, \omega)$	-2
$\sigma_{yxyx}^{(3)}(\omega, -\omega, \omega) + \sigma_{yyxx}^{(3)}(\omega, -\omega, \omega)$	-2
$\sigma_{yxxy}^{(3)}(\omega, -\omega, \omega)$	0
$\sigma_{xyyy}^{(3)}(\omega, -\omega, \omega)$	0
$\sigma_{xxxy}^{(3)}(\omega, -\omega, \omega) + \sigma_{xyxx}^{(3)}(\omega, -\omega, \omega)$	+1
$\sigma_{xxyx}^{(3)}(\omega, -\omega, \omega)$	-1
two-photon ( $-\omega \rightarrow \omega$ ) conductivity element(s)	value ( $\times g_0\eta\eta_x/E_0^2$ )
$\sigma_{yyyy}^{(3)}(\omega, \omega, -\omega)$	-1
$\sigma_{yxyx}^{(3)}(\omega, \omega, -\omega) + \sigma_{yyxx}^{(3)}(\omega, \omega, -\omega)$	-2
$\sigma_{yxxy}^{(3)}(\omega, \omega, -\omega)$	-1
$\sigma_{xyyy}^{(3)}(\omega, \omega, -\omega)$	+1
$\sigma_{xxxy}^{(3)}(\omega, \omega, -\omega) + \sigma_{xyxx}^{(3)}(\omega, \omega, -\omega)$	-2
$\sigma_{xxyx}^{(3)}(\omega, \omega, -\omega)$	+1

For the third-harmonic conductances, the splitting also holds for  $E_0 f(\phi, a, b) = f_A(\phi, a)E_y^3 + f_B(\phi, b)E_x^2E_y/2$ . We note that  $f_A(\phi, a)$  and  $f_B(\phi, b)$  are related to the conductivity tensor elements in the same way as above. We summarize the contributions to the third-harmonic conductivity tensor elements from the single-photon, two-photon, and three-photon transitions obtained from Eqs. (3b) and (4b) in Table II.

To simplify the discussion, in the following we present results for mGNR20, the metallic acGNR  $N = 20$  atoms wide, for an applied field strength  $E_0 = 10$  kV/m. From Eqs. (3) and (4), we see that illumination of an unbiased, infinitely-long mGNR by a THz harmonic electric field results in a nonlinear response that is strongly dependent on the polarization state of the applied field. Fig. 1 illustrates the polarization dependence of the longitudinal and transverse Kerr and third-harmonic nonlinear conductances at  $T = 0$  K and 300 K for intrinsic mGNR20.

For CW ( $\sigma_+$ ) and CCW ( $\sigma_-$ ) CP, *i.e.*,  $\phi = 45^\circ$  and  $135^\circ$ , the third-order conductances are antisymmetric. The shape of the conductance is a superposition of the contribution from

TABLE II. Third-harmonic conductivity tensor contributions

single-photon ( $-\omega/2 \rightarrow \omega/2$ ) conductivity component	value ( $\times g_0 \eta \eta_x / E_0^2$ )
$\sigma_{yyyy}^{(3')}$	+1/2
$\sigma_{yxyx}^{(3')} + \sigma_{yyxx}^{(3')} + \sigma_{yxxy}^{(3')}$	-1/12
$\sigma_{xyyy}^{(3')}$	-1/2
$\sigma_{xxyx}^{(3')} + \sigma_{xyxx}^{(3')} + \sigma_{xxxy}^{(3')}$	+5/12
two-photon ( $-\omega \rightarrow \omega$ ) conductivity component	value ( $\times g_0 \eta \eta_x / E_0^2$ )
$\sigma_{yyyy}^{(3')}$	-1
$\sigma_{yxyx}^{(3')} + \sigma_{yyxx}^{(3')} + \sigma_{yxxy}^{(3')}$	-5/3
$\sigma_{xyyy}^{(3')}$	+1
$\sigma_{xxyx}^{(3')} + \sigma_{xyxx}^{(3')} + \sigma_{xxxy}^{(3')}$	+1/3
three-photon ( $-3\omega/2 \rightarrow 3\omega/2$ ) conductivity component	value ( $\times g_0 \eta \eta_x / E_0^2$ )
$\sigma_{yyyy}^{(3')}$	+1/2
$\sigma_{yxyx}^{(3')} + \sigma_{yyxx}^{(3')} + \sigma_{yxxy}^{(3')}$	+7/4
$\sigma_{xyyy}^{(3')}$	-1/2
$\sigma_{xxyx}^{(3')} + \sigma_{xyxx}^{(3')} + \sigma_{xxxy}^{(3')}$	-7/4

Here  $\sigma_{\nu\alpha\beta\gamma}^{(3')}$  denotes  $\sigma_{\nu\alpha\beta\gamma}^{(3)}(\omega, \omega, \omega)$

the  $E_y$  and  $E_x$  components. The overall dependence of the third order current component  $J_\nu^{(3)}(\omega_0)$  is of the form [2, 30],

$$J_\nu^{(3)}(\omega_0) = g_\nu^{(3)}(\omega_0, \phi) E_0 = g_{\nu,A}(\omega_0) E_y + g_{\nu,B}(\omega_0) E_x \quad (5)$$

The first term,  $g_{\nu,A} \propto e^2 E_y^2 / (\hbar^2 \omega^4)$ , and agrees with [1, 2, 11, 12]. The second term,  $g_{\nu,B} \propto P_{circ}$  (see *e.g.* [18, 19]). Due to the current operator used, there is no analog of left or right handedness for the carriers in mGNR [32]. The direction of the *optically induced third order current* results from the interference between the local current density excited by the elliptical polarization of the field, or the radiation helicity  $P_{circ}$ , and the isospin of the carriers [1, 18, 20, 32]. Finally, for the LP cases  $\hat{y}$  and  $\hat{x}$ , ( $\phi = 0^\circ$  and  $\phi = 90^\circ$ ) respectively, contribution from the second term vanishes [20] and we recover the results reported previously [30]. In Fig. 2 we compare the longitudinal and transverse Kerr and

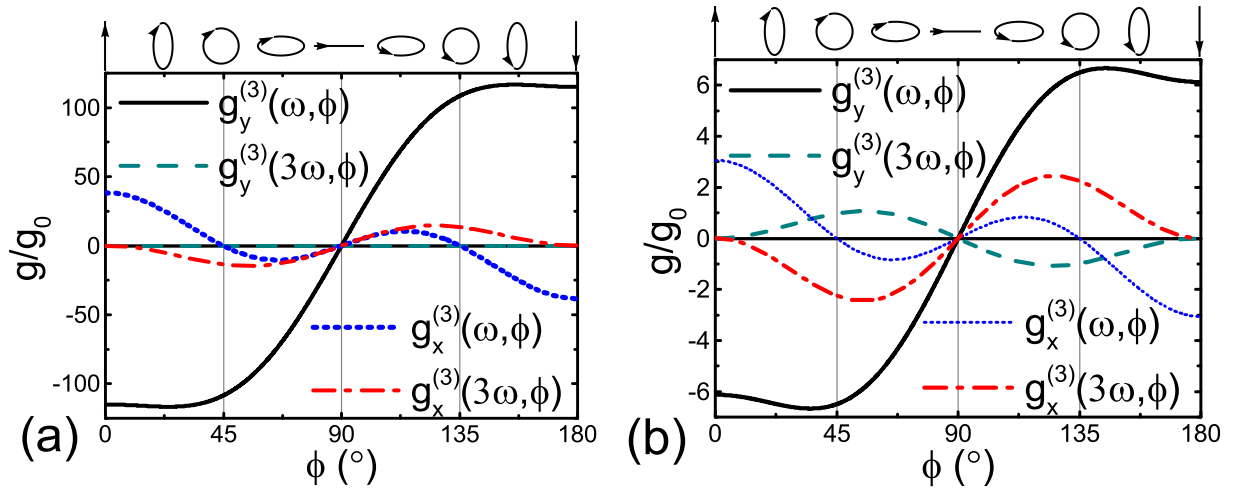


FIG. 1. Kerr and third-harmonic conductances of mGNR20 as a function of the incident THz electric field polarization state (see top inset) for: (a)  $T = 0$  K, and (b)  $T = 300$  K.  $f = 1$  THz,  $E_0 = 10$  kV/m.

third-harmonic conductances as a function of the Fermi level  $E_F$  at  $T = 0$  K. For  $E_F$  well below the optical phonon energy ( $\sim 200$  meV), and a 1 THz excitation frequency for a LP field in the  $\hat{y}$  direction ( $\phi = 0^\circ$ ) and  $\sigma_+$  CP ( $\phi = 45^\circ$ ) we see thresholding behavior of the nonlinear conductances for the direct interband transition at low temperature [30]. The three critical frequencies for  $E_F/h$ : 0.5 THz, 1 THz and 1.5 THz correspond to turning off the thermal distribution at  $\omega/2$ ,  $\omega$  and  $3\omega/2$  [30]. These frequencies are independent of the polarization states  $\phi$ , and are only functions of  $g_{\nu,A}(\omega_0)$  and  $g_{\nu,B}(\omega_0)$  in Eq. (5).

In the interest of brevity, we note briefly that the overall temperature dependence of all non-zero extrinsic conductances show that the nonlinearity persists even up to room temperature. Further, the curves asymptotically approach the intrinsic mGNR conductance for a given polarization state as the temperature increases. It is also interesting to note that the transverse Kerr conductances are identically zero for CP, independent of the Fermi level and temperature, in qualitative agreement with [29]. This may be understood as the cancellation of the contribution from  $E_y$  and  $P_{circ}$  in Eq. (4a) for CP.

Fig. 3 illustrates the excitation-frequency ( $2\pi f = \omega$ ) dependence of the Kerr and third-harmonic conductances for both  $\hat{y}$  LP ( $\phi = 0^\circ$ ) and  $\sigma_+$  CP ( $\phi = 45^\circ$ ) excitation fields in extrinsic mGNR20 ( $E_F/h = 0.7$  THz). At  $T = 0$  K (Figs. 3a and 3c) both CP Kerr



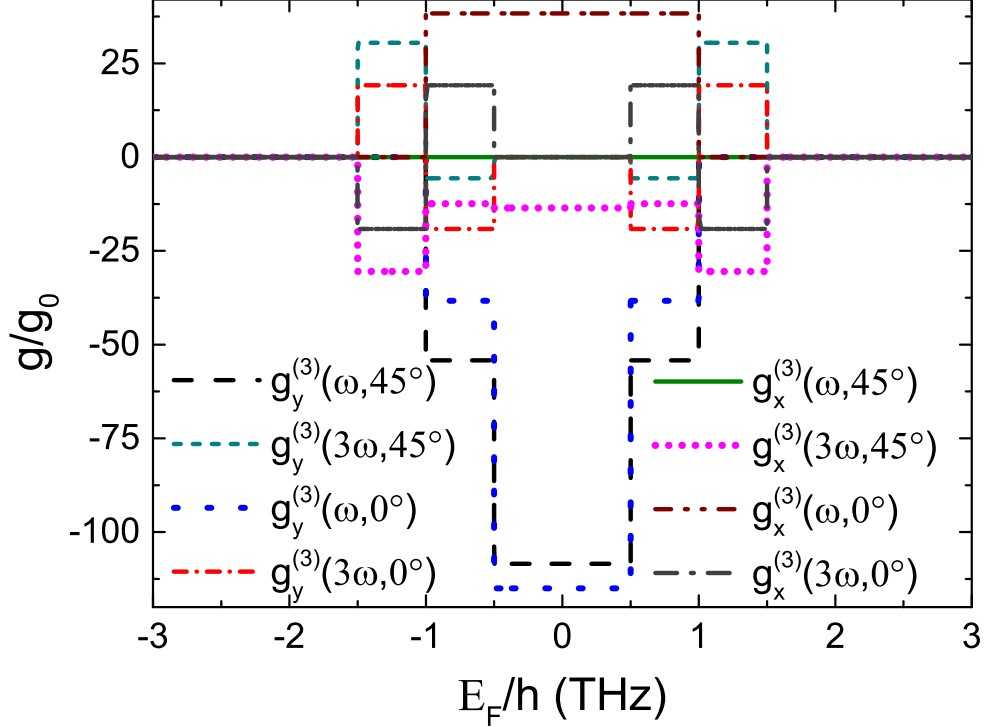


FIG. 2. Longitudinal and transverse components of the Kerr and third-harmonic conductances for extrinsic mGNR20 as a function of the Fermi level  $E_F$  and incident field polarization state. For this plot  $f = 1$  THz,  $E_0 = 10$  kV/m, and  $T = 0$  K.

conductance components behave in a manner qualitatively similar to the LP result for the longitudinal component of the conductance while the transverse component of the LP conductance is zero. However the CP third-harmonic conductances behave quite differently from their LP counterparts. Whereas the low-temperature LP conductance components are bandlimited (nonzero over  $2E_F/3h < f < 2E_F/h$ ), the transverse CP conductances *persist to significantly higher frequencies*, reducing to  $|g|/g_0 = 0.1$  at approximately 2.7 THz. At  $T = 300$  K (Figs. 3b and 3d), another behavior is noted: while the CP and longitudinal component of the LP Kerr conductance follow a similar decay envelope with increasing excitation frequency, both CP third-harmonic conductance components are *enhanced by nearly three orders of magnitude* over their LP counterparts at  $f = 1$  THz, and this enhancement persists to higher frequencies and is still nearly two orders of magnitude at  $f = 3$  THz. The enhancement for the transverse component of the CP third-harmonic conductance is observed to be slightly stronger than that for the longitudinal component of the CP third-harmonic conductance.

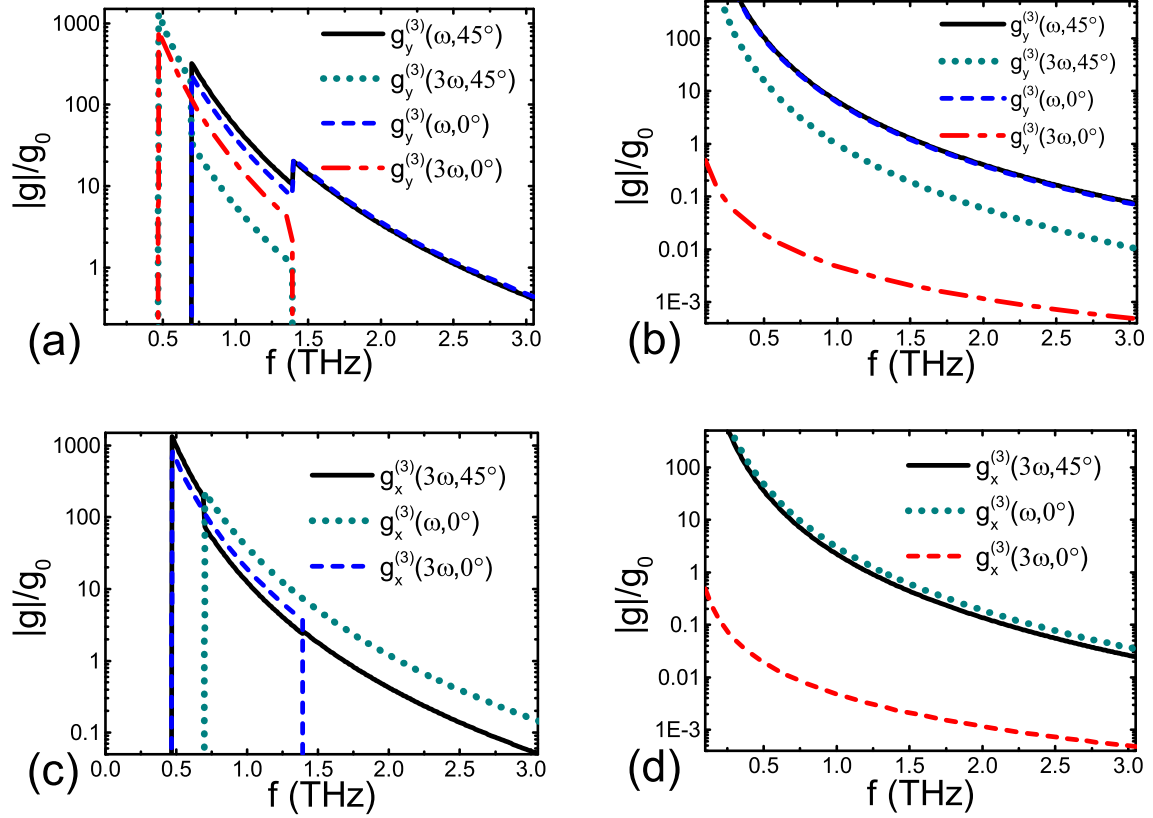


FIG. 3. Excitation frequency ( $2\pi f = \omega$ ) dependence of the components of nonlinear Kerr and third-harmonic conductances for extrinsic mGNR20 ( $E_F/h = 0.7$  THz): a) longitudinal conductance at  $T = 0$  K, b) longitudinal conductance at  $T = 300$  K, c) transverse conductance at  $T = 0$  K, and d) transverse conductance at  $T = 300$  K. For all plots,  $E_0 = 10$  kV/m. Note that for all temperatures, the CP transverse Kerr conductance is identically zero.

In conclusion, we report calculations describing the third-order nonlinear response of both intrinsic and extrinsic mGNR to an elliptically-polarized THz electric field. We show that the resulting Kerr conductances for extrinsic mGNR persist to significantly higher excitation frequencies at low temperature, and at room temperature, the CP third-harmonic conductances are enhanced by 2-3 orders of magnitude over their counterparts excited with only LP. Further, we describe the Fermi-level and temperature dependence of these nonlinearities. The enhancement in spectral range and magnitude for these nonlinearities suggests that they may exhibit wide applicability in THz devices excited with elliptically-polarized THz electric fields.

The recent synthesis of ultrathin mGNR with widths  $L_x < 10$  nm [33, 34], coupled with

the proposed experimental setup described in this letter, suggest that experimental measurement of the THz nonlinear response in thin mGNR should be possible at relatively low excitation field strengths. Notably, the enhancement of the third-order third-harmonic nonlinearity with small changes in Fermi level and applied CP excitation field at room temperature indicates that mGNR may provide the basis for developing a sensitive graphene-based detector, broadband modulator, or source over a wide range of temperatures.

- 
- [1] M. M. Glazov and S. D. Ganichev, *Physics Reports* **535**, 101 (2014).
  - [2] A. R. Wright, X. G. Xu, J. C. Cao, and C. Zhang, *Appl. Phys. Lett.* **95**, 072101 (2009).
  - [3] E. Hendry, P. J. Hale, J. Moger, A. K. Savchenko, and S. A. Mikhailov, *Phys. Rev. Lett.* **105**, 097401 (2010).
  - [4] S. Das Sarma, S. Adam, E. H. Hwang, and E. Rossi, *Rev. Mod. Phys.* **83**, 407 (2011).
  - [5] M. M. Glazov, *JETP Letters* **93**, 366 (2011).
  - [6] I. Maeng, S. Lim, S. J. Chae, Y. H. Lee, H. Choi, and J.-H. Son, *Nano Lett.* **12**, 551 (2012).
  - [7] T. Gu, N. Petrone, J. F. McMillan, A. van der Zande, M. Yu, G.-Q. Lo, D. L. Kwong, J. Hone, and C. W. Wong, *Nat. Photonics* **6**, 554 (2012).
  - [8] M. Gullans, D. E. Chang, F. H. L. Koppens, F. J. Garcia deAbajo, and M. D. Lukin, *Phys. Rev. Lett.* **111**, 247401 (2013).
  - [9] N. Kumar, J. Kumar, C. Gerstenkorn, R. Wang, H.-Y. Chiu, A. L. Smirl, and H. Zhao, *Phys. Rev. B* **87**, 121406 (2013).
  - [10] H. A. Hafez, I. Al-Naib, M. M. Dignam, Y. Sekine, K. Oguri, F. Blanchard, D. G. Cooke, S. Tanaka, F. Komori, H. Hibino, and T. Ozaki, *Phys. Rev. B* **91**, 035422 (2015).
  - [11] J. L. Cheng, N. Vermeulen, and J. E. Sipe, *Phys. Rev. B* **92**, 235307 (2015).
  - [12] S. A. Mikhailov, *Phys. Rev. B* **93**, 085403 (2016).
  - [13] D. S. L. Abergel, V. Apalkov, J. Berashevich, K. Ziegler, and T. Chakraborty, *Adv. Phys.* **59**, 261 (2010).
  - [14] V. G. Kravets, A. N. Grigorenko, R. R. Nair, P. Blake, S. Anissimova, K. S. Novoselov, and A. K. Geim, *Phys. Rev. B* **81**, 155413 (2010).
  - [15] T. Oka and H. Aoki, *Phys. Rev. B* **79**, 081406 (2009).
  - [16] J. Karch, P. Olbrich, M. Schmalzbauer, C. Zoth, C. Brinsteiner, M. Fehrenbacher, U. Wurst-

- bauer, M. M. Glazov, S. A. Tarasenko, E. L. Ivchenko, D. Weiss, J. Eroms, S. Yakimova, S. Lara-Avila, S. Kubatkin, and S. D. Ganichev, *Phys. Rev. Lett.* **105**, 227402 (2010).
- [17] C. Jiang, V. A. Shalygin, V. Y. Panevin, S. N. Danilov, M. M. Glazov, R. Yakimova, S. Lara-Avila, S. Kubatkin, and S. D. Ganichev, *Phys. Rev. B* **84**, 125429 (2011).
- [18] J. Karch, P. Olbrich, M. Schmalzbauer, C. Brinsteiner, U. Wurstbauer, M. M. Glazov, S. A. Tarasenko, E. L. Ivchenko, D. Weiss, J. Eroms, and S. D. Ganichev, arXiv preprint arXiv:1002.1047 (2010).
- [19] J. Karch, C. Drexler, P. Olbrich, M. Fehrenbacher, M. Hirmer, M. M. Glazov, S. A. Tarasenko, E. L. Ivchenko, B. Birkner, J. Eroms, D. Weiss, R. Yakimova, S. Lara-Avila, S. Kubatkin, M. Ostler, T. Seyller, and S. D. Ganichev, *Phys. Rev. Lett.* **107**, 276601 (2011).
- [20] Y. Liu, G. Bian, T. Miller, and T.-C. Chiang, *Phys. Rev. Lett.* **107**, 166803 (2011).
- [21] S. A. Sørngård, S. I. Simonsen, and J. P. Hansen, *Phys. Rev. A* **87**, 053803 (2013).
- [22] L. Brey and H. A. Fertig, *Phys. Rev. B* **73**, 235411 (2006).
- [23] L. Brey and H. A. Fertig, *Phys. Rev. B* **75**, 125434 (2007).
- [24] D. R. Andersen and H. Raza, *Phys. Rev. B* **85**, 075425 (2012).
- [25] W. Liao, G. Zhou, and F. Xi, *J. Appl. Phys.* **104**, 126105 (2008).
- [26] Z. Duan, W. Liao, and G. Zhou, *Advances in Condensed Matter Physics* **2010**, 258019 (2010).
- [27] K. I. Sasaki, K. Kato, Y. Tokura, K. Oguri, and T. Sogawa, *Phys. Rev. B* **84**, 085458 (2011).
- [28] Z. Gu, H. A. Fertig, D. P. Arovas, and A. Auerbach, *Phys. Rev. Lett.* **107**, 216601 (2011).
- [29] H. L. Calvo, P. M. Perez-Piskunow, H. M. Pastawski, S. Roche, and L. E. F. F. Torres, *J. Phys.: Condens. Matter* **25**, 144202 (2013).
- [30] Y. Wang and D. R. Andersen, *Phys. Rev. B* **93**, 235430 (2016).
- [31] Y. Wang and D. R. Andersen, *IEEE J. Sel. Topics Quantum Electron.* doi:10.1109/JSTQE.2016.2564402 (in press).
- [32] C. W. J. Beenakker, *Rev. Mod. Phys.* **80**, 1337 (2008).
- [33] A. Kimouche, M. M. Ervasti, R. Drost, S. Halonen, A. Harju, P. M. Joensuu, J. Sainio, and P. Liljeroth, *Nat. Commun.* **6**, 10177 (2015).
- [34] R. M. Jacobberger, B. Kiraly, M. Fortin-Deschenes, P. L. Levesque, K. M. McElhinny, G. J. Brady, R. R. Delgado, S. S. Roy, A. Mannix, M. G. Lagally, P. G. Evans, P. Desjardins, R. Martel, M. C. Hersam, N. P. Guisinger, and M. S. Arnold, *Nat. Commun.* **6**, 10177 (2015).